

# Chemical enrichment in very low-metallicity environments: Boötes I

Donatella Romano,<sup>1\*</sup> Michele Bellazzini,<sup>1</sup> Else Starkenburg,<sup>2,†</sup> and Ryan Leaman<sup>3,4</sup>

<sup>1</sup>INAF, Osservatorio Astronomico di Bologna, Via Ranzani 1, I-40127 Bologna, Italy

<sup>2</sup>Department of Physics and Astronomy, University of Victoria, PO Box 3055 STN CSC, Victoria, BC V8W 3P6, Canada

<sup>3</sup>Instituto de Astrofísica de Canarias, E-38205 La Laguna, Tenerife, Spain

<sup>4</sup>Departamento de Astrofísica, Universidad de La Laguna, E-38205 La Laguna, Tenerife, Spain

Accepted 2014 November 13. Received 2014 November 5; in original form 2014 July 29

## ABSTRACT

We present different chemical evolution models for the ultrafaint dwarf galaxy Boötes I. We either assume that the galaxy accretes its mass through smooth infall of gas of primordial chemical composition (*classical* models) or adopt mass accretion histories derived from the combination of merger trees with semi-analytical modelling (*cosmologically-motivated* models). Furthermore, we consider models with and without taking into account inhomogeneous mixing in the ISM within the galaxy, i.e. *homogeneous* versus *inhomogeneous* models. The theoretical predictions are then compared to each other and to the body of the available data. From this analysis, we confirm previous findings that Boötes I has formed stars with very low efficiency but, at variance with previous studies, we do not find a clear-cut indication that supernova explosions have sustained long-lasting galactic-scale outflows in this galaxy. Therefore, we suggest that external mechanisms such as ram pressure stripping and tidal stripping are needed to explain the absence of neutral gas in Boötes I today.

**Key words:** galaxies: abundances – galaxies: dwarf – galaxies: evolution – galaxies: individual (Boötes I) – stars: abundances.

## 1 INTRODUCTION

Since its recent discovery (Belokurov et al. 2006), the Boötes I ultrafaint dwarf spheroidal galaxy (UFD) has been the subject of a number of investigations, aiming at providing insight into the formation and evolution of this system. Located at  $66 \pm 2$  kpc distance from the Sun and with an absolute visual magnitude of  $M_V = -6.3 \pm 0.2$  mag (McConnachie 2012), Boötes I is one of the brightest UFDs found lurking around the Milky Way, and one of its closest satellites. The color-magnitude diagrams reveal that its stellar population is old and metal-poor, with age spread (if any) limited to a few billion years (de Jong et al. 2008; Hughes, Wallerstein & Bossi 2008). No H I is detected in or around Boötes I to a  $3\sigma$  upper limit of  $180 M_\odot$  within the optical half-light radius; the resulting H I mass-to-light ratio is, thus, extremely low, less than  $0.002 M_\odot/L_\odot$ , which makes it one of the most gas-poor galaxies known (Bailin & Ford 2007). Whichever mechanisms are responsible for gas removal from Boötes I, the absence of gas streams or outflowing gas suggests that they have completed long ago. Boötes I also exhibits extremely irregular density contours (Belokurov et al. 2006), which indicates that it is undergoing tidal disruption.

Estimates of the dynamical mass enclosed within the half-light radius ( $r_h = 242 \pm 21$  pc; McConnachie 2012) have suggested that this extremely low-luminosity system is possibly the darkest Milky

Way satellite, with  $M_{\text{dyn}}(\leq r_h) = 2.36 \times 10^7 M_\odot$ , when a stellar velocity dispersion of  $\sigma_v = 9.0 \text{ km s}^{-1}$  is adopted (Wolf et al. 2010). However, large uncertainties affect this determination and the mass may be sensibly smaller, with a lower limit of  $8.1 \times 10^5 M_\odot$  reported by McConnachie (2012), based on Koposov et al.’s (2011) lower value for  $\sigma_v$ . Koposov et al. actually find two kinematically distinct stellar components in Boötes I: a dominant, ‘cold’ component, that encompasses 70 per cent of the member stars and has a low projected radial velocity dispersion of  $2.4^{+0.9}_{-0.5} \text{ km s}^{-1}$ , and a minority, ‘hot’ component, that encompasses 30 per cent of the member stars and has a projected radial velocity dispersion of about  $9 \text{ km s}^{-1}$ . They speculate that this may arise from the velocity anisotropy of the stellar population.

Despite its small baryonic mass (the stellar mass is only  $2.9 \times 10^4 M_\odot$ , assuming a stellar mass-to-light ratio of 1; McConnachie 2012), Boötes I shows a large star-to-star variation in Fe abundances (Norris et al. 2008, 2010a; Feltzing et al. 2009; Lai et al. 2011; Gilmore et al. 2013), in starkly sharp contrast with the lack of evidence for [Fe/H] dispersion in Galactic globular clusters of similar mass (see the review by Gratton, Sneden & Carretta 2004 and Carretta et al. 2009). Iron abundances [Fe/H] ranging from  $-3.7$  to  $-1.65$  in Boötes I clearly point to self-enrichment from essentially primordial initial chemical composition and provide indirect evidence for the presence of dark matter (Norris et al. 2008) or, alternatively, for a baryonic mass at the epoch of chemical enrichment significantly higher than seen today.

Recently, Vincenzo et al. (2014) modelled the chemical evo-

\* E-mail: donatella.romano@oabo.inaf.it

† CIFAR Global Scholar.

**Table 1.** High-resolution abundances of Boötes I stars.

Star	[Fe/H]	$\sigma$	[C/Fe]	$\sigma$	[Na/Fe]	$\sigma$	[Mg/Fe]	$\sigma$	[Ca/Fe]	$\sigma$	[Ti/Fe]	$\sigma$	[Ba/Fe]	$\sigma$	Source/Instr. <sup>a</sup>
Boo-7	-2.33	0.05					0.41	0.11	0.23	0.11			-0.75		1/H
Boo-9	-2.64	0.14	< -0.29		0.01	0.27	0.13	0.16	0.18	0.05	0.26	0.10	-0.89	0.27	3/S
Boo-33	-2.52	0.07					0.45	0.17	0.40	0.14			-0.40	0.18	1/H
	-2.32	0.16			0.05	0.23	0.26	0.22	0.14	0.06	-0.02	0.17	-0.40	0.19	2/U
Boo-41	-1.88	0.16					0.50	0.22	0.28	0.06	0.78	0.20	-0.39	0.20	2/U
Boo-94	-2.95	0.04					0.49	0.05	0.22	0.05					1/H
	-2.94	0.16			0.15	0.20	0.49	0.16	0.30	0.06	0.26	0.13	-0.94	0.20	2/U
	-3.18	0.14	<0.25		-0.32	0.20	0.39	0.06	0.46	0.05	0.28	0.19	-0.80	0.12	3/S
Boo-117	-2.29	0.06					0.35	0.15	0.29	0.15			-0.46	0.10	1/H
	-2.18	0.16			-0.05	0.24	0.18	0.22	0.20	0.06	0.14	0.13	-0.65	0.25	2/U
	-2.15	0.18	-0.79	0.35	-0.25	0.08	0.04	0.14	0.01	0.13	0.23	0.17	-0.43	0.10	3/S
Boo-119	-3.33	0.16			0.73	0.23	1.04	0.22	0.46	0.18	0.80	0.28	-1.00	0.24	2/U
Boo-121	-2.44	0.04					0.37	0.16	0.38	0.14			-0.43		1/H
	-2.49	0.19	< -0.24		-0.25	0.10	0.20	0.20	0.24	0.08	0.09	0.19	-0.63	0.20	3/S
Boo-127	-2.03	0.06					0.71	0.09	0.02	0.10			-0.64	0.31	1/H
	-2.01	0.16					0.17	0.18	0.16	0.05	0.20	0.14	-0.69	0.29	2/U
	-1.92	0.21	-0.77	0.36	-0.18	0.15	0.11	0.07	0.19	0.10	0.15	0.15	-0.87	0.24	3/S
Boo-130	-2.32	0.16			0.03	0.21	0.21	0.22	0.19	0.08	0.17	0.16	-0.54	0.23	2/U
Boo-911	-2.26	0.05					0.29	0.13	0.40	0.06			-0.56	0.08	1/H
	-2.16	0.23	-0.77	0.37	-0.28	0.08	0.35	0.13	-0.01	0.12	-0.09	0.11	-0.64	0.15	3/S
Boo-1137 <sup>b</sup>	-3.66	0.11	0.26	0.2	-0.08	0.14	0.30	0.21	0.55	0.14	0.48	0.10	-0.55	0.17	2/U

Notes. Identification system by Norris et al. (2008). Solar reference values from Asplund et al. (2009).

<sup>a</sup> 1: Feltzing et al. 2009; 2: Gilmore et al. 2013; 3: Ishigaki et al. 2014; H: High Resolution Echelle Spectrometer (HIRES) on Keck I; U: Ultraviolet and Visual Echelle Spectrograph (UVES) on VLT; S: High Dispersion Spectrograph (HDS) on Subaru.

<sup>b</sup> [Fe/H], [Mg/Fe], [Ca/Fe] and [Ti/Fe] from Table 8 of Gilmore et al. (2013); [C/Fe], [Na/Fe] and [Ba/Fe] from Table 2 of Norris et al. (2010b), placed on the Asplund et al. (2009) scale.

lution of Boötes I and concluded that this galaxy experienced very low star formation activity and efficient galactic winds, that got rid of all its gas. Their findings are in agreement with previous claims by Salvadori & Ferrara (2009) that UFDs have formed stars very ineffectively, turning less than 3 per cent of their baryons into stars.

All its characteristics make Boötes I an outstanding local benchmark of the elusive earliest stages of galaxy formation. The purpose of this paper is to interpret the chemical features of stars in Boötes I in terms of enrichment time-scales and early evolutionary conditions. In Section 2, we review the available spectroscopic data. In Section 3, we present our chemical evolution models. In Section 4 our results are discussed, in comparison to the observations. Finally, in Section 5 some conclusions are drawn.

## 2 OBSERVATIONAL DATA

### 2.1 Low- and high-resolution spectroscopy

Nowadays, it is widely recognized that the relative distribution of the chemical elements inside galaxies and the spread in abundance ratios are major diagnostics of structure formation and evolution. Reliable abundance determinations of a large number of chemical species are best obtained by means of high spectral resolution analyses. However, high-resolution spectroscopic measurements of individual members of the faintest Milky Way companions are extremely challenging. At low resolution, the exposure times significantly shorten and larger samples of stars can be probed. However, from low-resolution spectra typically only iron,  $\alpha$  elements and carbon abundances can be obtained. Medium-resolution spectroscopy ( $R \sim 6000$ ) offers a reasonable trade-off, especially if coupled to multi-object capability, by enabling valuable data to be collected

for thousands of stars in Milky Way satellites (e.g. Battaglia et al. 2006; Kirby et al. 2010; Vargas et al. 2013). In the following, we review the spectroscopic data available for the Boötes I UFD.

Lai et al. (2011) have presented a chemical abundance analysis of 25 members of Boötes I. Target stars were selected from the radial velocity survey of Martin et al. (2007) and observed with the Low Resolution Imaging Spectrometer (LRIS; Oke et al. 1995) mounted on the Keck I telescope. The resolving power is  $R \sim 1800$  at 5100 Å. The data allow measurements of [Fe/H], [C/Fe] and [ $\alpha$ /Fe] for each star. A significant spread in metallicity (2.1 dex in [Fe/H]) and a low mean iron abundance ( $\langle$ [Fe/H] $\rangle = -2.59$  dex) are found, matching previous estimates (see next paragraph). The authors caution that a systematic offset on the order  $-0.13$  dex from literature values is likely present in their [ $\alpha$ /Fe] ratios.

High-resolution spectroscopic studies have been carried out for sparse samples of Boötes I stars, using different instrumentation (see Table 1). Feltzing et al. (2009) have found a mean metallicity of  $-2.3$  dex for seven red giant stars with individual [Fe/H] values ranging from  $-2.9$  to  $-1.9$  dex. One star in their sample, Boo-127, shows an unusually high [Mg/Ca] ratio, similarly to Dra-119 in Draco (Fulbright et al. 2004) and Her-2 and Her-3 in Hercules (Koch et al. 2008). The high value of [Mg/Fe] for Boo-127, however, is not confirmed by Gilmore et al. (2013), who, on the other hand, find excellent abundance agreement for Ca, Ba and Fe for the four stars they have in common with Feltzing et al. (2009). One star in Gilmore et al.'s (2013) sample, Boo-41, displays an anomalously high Ti abundance. Another object, Boo-119, is a carbon-enhanced metal poor star ([Fe/H] =  $-3.33$  dex) with no neutron-capture element enhancement (CEMP-no star) and [Mg/Fe] = 1.04 dex. If both these stars are excluded, a weak signature of declining [ $\alpha$ /Fe] with increasing [Fe/H] is found, in contrast to what is known for field

halo stars of the same metallicities (see also Vargas et al. 2013). The chemical evolution of Boötes I is suggested to have proceeded in a homogeneous manner, at variance with Feltzing et al. (2009), who support the presence of inhomogeneities. In order to shed light on these discrepancies, Ishigaki et al. (2014) have recently performed an independent analysis of six red giant stars in Boötes I. They have five stars and three stars, respectively, in common with Feltzing et al. (2009) and Gilmore et al. (2013). Their analysis does not support a highly inhomogeneous chemical evolution for Boötes I and suggests a low value for  $[\text{Mg}/\text{Fe}]$  in Boo-127, fully consistent with Gilmore et al. (2013) and in disagreement with Feltzing et al. (2009). Finally, carbon abundances from medium-resolution spectra for sixteen Boötes I red giants are presented in Norris et al. (2010a). The spread in carbon abundances is large,  $\Delta[\text{C}/\text{H}] = 1.5$  dex.

For the purpose of the present work, we adopt the high-resolution data published in Feltzing et al. (2009), Norris et al. (2010b), Gilmore et al. (2013) and Ishigaki et al. (2014) (see Table 1, where the ratios have been adjusted using Asplund et al. 2009 solar reference values if needed). Moreover, we adopt carbon abundances by Norris et al. (2010a) and Lai et al. (2011) for sixteen stars and one star (Boo-119), respectively. These abundances have been inferred from medium- and low-resolution spectra and are not listed in Table 1. To ensure a good statistic, we also use as a constraint the Boötes I ‘combined’ metallicity distribution function (MDF) obtained by Lai et al. (2011) by expanding their sample to include non-overlapping stars from Norris et al. (2010a) and Feltzing et al. (2009); the resulting empirical distribution totals 41 stars.

### 3 CHEMICAL EVOLUTION MODELS

We compute the evolution of the abundances of several chemical elements (H, D, He, Li, C, N, O, Na, Mg, Al, Si, S, Ca, Sc, Ti, Cr, Mn, Co, Ni, Fe, Cu, Zn) in the interstellar medium (ISM) of Boötes I. We use detailed numerical models, that solve the classical set of equations of chemical evolution (see e.g. Tinsley 1980; Pagel 1997; Matteucci 2001, 2012).

#### 3.1 Classical models

Our *classical* models rest on the following assumptions:

- (i) inflow of gas of primordial chemical composition provides the raw material for star formation;
- (ii) galactic outflows remove gas from the system;
- (iii) the stellar initial mass function (IMF) is constant in space and time;
- (iv) the finite stellar lifetimes are taken into account (no *instantaneous recycling approximation*, IRA, is adopted).

##### 3.1.1 Gas accretion and star formation

For the sake of simplicity, the rate of gas infall is parametrized as

$$\frac{d\mathcal{M}_b}{dt} \propto e^{-t/\tau}, \quad (1)$$

where  $\mathcal{M}_b$ , the total amount of matter ever accreted, and  $\tau$ , the e-folding time-scale, are free parameters of the models. A smooth accretion of gas is clearly a rough approximation of the true assembly history of galaxies. According to modern theories of galaxy formation, in fact, the mass assembly must proceed through discrete

episodes and mergers play a key role (see e.g. Conselice 2012, for a recent review). However, if most of the mass is gathered early on in gaseous subclumps and the stars form mostly *in situ*, the chemical properties predicted for the bulk of the stellar population are expected to be quite robust against the simplified mass assembly history implied by Equation (1).

The gas is turned into stars following a Kennicutt-Schmidt law (Schmidt 1959; Kennicutt 1998):

$$\psi(t) = \nu \mathcal{M}_{\text{gas}}(t), \quad (2)$$

where  $\nu$ , the efficiency of the process, is a free parameter of the models. To be precise, the original Kennicutt (1998) law refers to surface densities:  $\dot{\Sigma}_* \propto \Sigma_{\text{gas}}^{1.4 \pm 0.15}$ . For star-forming regions with roughly constant scale heights, the surface densities can be turned into volume densities:  $\dot{\rho}_* \propto \rho_{\text{gas}}^{1.5}$ . By assuming that the Kennicutt-Schmidt law indicates that the star formation rate is controlled by the self-gravity of the gas, one can write:  $\dot{\rho}_* = \varepsilon \rho_{\text{gas}} / t_{\text{ff}}$ , where  $t_{\text{ff}} \propto 1/\sqrt{\rho_{\text{gas}}}$  and  $\varepsilon$  is a free parameter. We adopt this formulation of the star formation rate, with  $\nu = \varepsilon / t_{\text{ff}}$ . We do not consider a gas density threshold for star formation. As for the stellar IMF, we adopt a Kroupa (2001) IMF in the mass range 0.1–100  $M_{\odot}$ , unless otherwise stated.

##### 3.1.2 Mechanical feedback

Thermal feedback from stars is included by assuming that type II and type Ia supernovae (SNe II and SNe Ia, respectively) deposit  $E_{\text{SN}} = 10^{51}$  erg of energy each<sup>1</sup> into the ISM. The energy injected by a typical massive star via stellar winds during its lifetime ( $E_{\text{wind}} = 10^{49}$  erg; see Gibson 1994, his figure 1) is added though it has a negligible effect on the global energy budget. In order to account for radiative energy losses, we assume constant values of the thermalization efficiencies,  $\varepsilon_{\text{SNII}} = \varepsilon_{\text{SNIa}} = \varepsilon_{\text{wind}} = \varepsilon = 0.01\text{--}0.1$  (see Table 2). It is worth stressing that there is not general consensus about these values in the literature (see e.g. Recchi 2014, for a recent review). Furthermore, the heating efficiency is likely to be a time-dependent quantity (Melioli & de Gouveia Dal Pino 2004).

At each time step, we compute the gas thermal and binding energies following Bradamante, Matteucci & D’Ercole (1998). When the thermal energy of the gas exceeds its binding energy, an outflow develops and the thermal energy of the gas is reset to zero. The rate of gas loss through the outflow is assumed to be proportional to the star formation rate

$$\frac{d\mathcal{M}_{\text{out}}}{dt} = w \psi(t), \quad (3)$$

where  $w$  is a further free parameter of the models describing the efficiency of the galactic wind. Following both theoretical and empirical considerations (e.g. Vader 1986, 1987; Recchi, Matteucci & D’Ercole 2001; Martin, Kobulnicky & Heckman 2002) we assume a higher ejection efficiency for the heavy elements freshly synthesised in SN explosions than for the neutral ISM (*selective winds*; Marconi, Matteucci & Tosi 1994); in particular, we assume  $w_{\text{heavy}} = 2 w_{\text{H,He}} = 12$ .

The final fate of the swept-up gas and supernova ejecta is matter of debate. Silich & Tenorio-Tagle (1998) find that the gas remains bound in the hot gaseous halos surrounding galaxies as massive as  $10^9\text{--}10^{10} M_{\odot}$ . A similar conclusion is reached by Marcolini et al. (2006) for lower mass galaxies (they analyse the specific

<sup>1</sup> The consequences of the occurrence of hypernovae with more energetic outputs are not explored.

**Table 2.** Parameters and final properties of the classical homogeneous models.

Model	$\mathcal{M}_b$ ( $M_\odot$ )	$\tau$ (Myr)	$\nu$ ( $\text{Gyr}^{-1}$ )	$\Delta t_{\text{SF}}$ (Gyr)	$r_h/r_{\text{DM}}$	$\mathcal{M}_{\text{DM}}$ ( $M_\odot$ )	$\varepsilon$	$w_{\text{heavy}}$	$\mathcal{M}_{\text{stars}}$ ( $10^4 M_\odot$ )	$\langle [\text{Fe}/\text{H}] \rangle_{\text{stars}}$ (dex)	$\Delta t_{\text{out}}$ (Myr)	$\mathcal{M}_{\text{gas}}$ ( $10^6 M_\odot$ )	Flag
Boo 1	$2 \times 10^6$	50	0.02	1	0.1	$2 \times 10^6$	0.01	12	1.5	-2.24	285	1.87	D
Boo 2	$2 \times 10^6$	50	0.02	1	0.1	$2 \times 10^6$	0.1	12	1.5	-2.25	45	1.74	
Boo 3	$2 \times 10^6$	50	0.02	1	—	—	0.01	12	1.5	-2.24	275	1.87	
Boo 4	$2 \times 10^6$	50	0.04	1	0.1	$2 \times 10^6$	0.01	12	3.0	-1.92	155	1.84	
Boo 5	$1.1 \times 10^7$	50	0.013	1	0.1	$1.1 \times 10^8$	0.1	12	5.5	-2.44	310	10.4	D
Boo 6	$1.1 \times 10^7$	50	0.026	0.5	0.1	$1.1 \times 10^8$	0.1	12	5.5	-2.52	165	10.4	
Boo 7	$1.1 \times 10^7$	50	0.053	0.25	0.1	$1.1 \times 10^8$	0.01	12	5.5	-2.60	—	10.4	
Boo 8 <sup>a</sup>	$1.1 \times 10^7$	50	0.053	0.25	0.1	$1.1 \times 10^8$	0.01	12	5.5	-2.60	—	10.4	
	$10^5$	50	4.0	0.02	0.1	$1.1 \times 10^8$	0.01	12	0.25	-2.46	15	0.09	
Boo 9	$1.1 \times 10^7$	50	0.013	1	0.1	$6.5 \times 10^7$	0.1	12	5.5	-2.44	280	10.3	

Notes. Listed in columns 1 to 13 are: the model name; the total baryonic (gaseous) mass accreted by the system; the infall time-scale; the star formation efficiency; the duration of the star formation episode; the ratio of the effective-to-dark matter core radius; the total dynamical mass of the system; the thermalization efficiency from SNe of all types and stellar winds; the efficiency of metal removal from the star forming regions; the final stellar mass of the system; the average stellar metallicity; the time interval between the beginning of star formation and the onset of the first episode of gas removal from the star forming region (that does not necessarily lead to gas removal from the system); the final gaseous mass of the system. A capital ‘D’ in the last column denotes whether the energy output from SNe exceeds the binding energy of the galaxy (which results in disrupting the object).

<sup>a</sup> This model is characterized by two bursts of star formation. The model parameters (columns 2–9) and final properties (columns 10–13) corresponding to the two distinct star formation episodes are listed in distinct rows.

case of Draco, a classical dwarf spheroidal galaxy of the Local Group). In this picture, gas removal ultimately results from ram pressure stripping (Mori & Burkert 2000) and/or tidal interaction with the Milky Way (Mayer et al. 2006). We note that our more massive models have low circular velocity,  $V_c = 14 \text{ km s}^{-1}$ ,<sup>2</sup> and virial temperature below  $10^4 \text{ K}$ . In such conditions, gas cools inefficiently (Sutherland & Dopita 1993). The cooling time is expected to be (slightly) lower than the (outflow) time and the material entrained in the outflow can possibly leave the galaxy (see Wang 1995). Clearly, the arguments above suffer of important oversimplifications –for instance, we do not take into account the role of gas geometry on the development of galactic winds (the interested reader is referred to Recchi & Hensler 2013 for a recent reappraisal of this problem). For the purpose of the present work, it suffices to say that in the framework of our classic chemical evolution models the gas entrained in the outflow is assumed to never re-enter the star-forming regions. Sawala et al. (2010, 2014) provide a more realistic treatment of the gas in dwarf galaxies with a range of masses that partly overlaps the one analysed here.

### 3.1.3 Chemical feedback

One of the most important ingredients of chemical evolution models are, of course, the stellar yields. In this work, we test two different grids of yields for both low- and intermediate-mass stars ( $1 \leq m/M_\odot \leq 8$ ) and massive stars ( $m > 8 M_\odot$ ):

(i) the metallicity-dependent yields from van den Hoek & Groenewegen (1997) for single low- and intermediate-mass stars and those from Woosley & Weaver (1995, their case B) for core-collapse SNe (our standard choice);

(ii) the metallicity-dependent yields from Karakas (2010) for

<sup>2</sup> Following Desai et al. (2004), this corresponds to a stellar central velocity dispersion  $\sigma_v = 9 \text{ km s}^{-1}$ , that agrees well with the observed values ( $2.4\text{--}9.0 \text{ km s}^{-1}$ , depending on the considered component, see Koposov et al. 2011).

single low- and intermediate-mass stars and those from Kobayashi et al. (2006) for core-collapse SNe.

Both grids of yields allow to reproduce reasonably well most of the abundance data for solar neighbourhood stars (see Romano et al. 2010). In Section 4 we show the results of the models with our standard choice of stellar yields. The impact of adopting different nucleosynthesis prescriptions is discussed in Appendix A. The yields for SNe Ia are always taken from Iwamoto et al. (1999, their model W7). The rate of SNe Ia is computed following the recipes outlined in Matteucci & Greggio (1986).

The adopted values of the parameters for our classical models are listed in columns 2 to 9 of Table 2.

### 3.2 Cosmologically-motivated models

In the classical chemical evolution modelling scheme described in the previous section, Boötes I is assumed to form via accretion of gaseous matter of primordial chemical composition, following (rather arbitrarily) a time-decaying infall rate. Possible interactions with the surroundings are not taken into account. However, nowadays the formation sites of even the smallest Milky Way satellites are directly resolved in large cosmological  $N$ -body dark matter simulations. This enables us to study the formation and evolution of Boötes I in a  $\Lambda$  cold dark matter ( $\Lambda$ CDM) universe.

We rest on recent work by Starkenburg et al. (2013), who combined six high-resolution Aquarius dark matter simulations (see Springel et al. 2008) with a semi-analytic model of galaxy formation (Li, De Lucia & Helmi 2010, that is in turn build upon Kauffmann et al. 1999; Springel et al. 2001; De Lucia, Kauffmann & White 2004; Croton et al. 2006; De Lucia & Blaizot 2007; De Lucia & Helmi 2008) to investigate the properties of the satellites of Milky Way-like galaxies in a fully cosmological setting (see also, e.g., Cooper et al. 2010; Font et al. 2011; De Lucia et al. 2014, for work on satellites based on the Aquarius Project). In their simulations, new prescriptions are included to follow stellar stripping and tidal disruption of satellites. While the main focus is on the star formation histories of dwarf galaxies in and around the Milky Way,

the treatment of chemical enrichment has some limitations due to the adoption of IRA.

For the purpose of the present work, we identify Boötes I analogues in the mock galaxy catalogue of Starkenburg et al. (2013), based on rather loose selection criteria: (i) *V*-band magnitude between  $-6.0$  and  $-6.5$  mag; (ii) mostly old stellar populations (more than 80 per cent of the stars are older than 10 Gyr); (iii) the galaxy is a satellite of the Milky-Way-like halo and no further out than 150 kpc today. We adopt the mass assembly and star formation histories of the Boötes I candidates and apply the post-processing technique described in Romano & Starkenburg (2013) in order to obtain the detailed chemical composition of synthetic Boötes I stars in a fully cosmological framework. We find that for such a small galaxy not all cosmological models are suitable for this post-processing scheme. This is at least partly due to the assumption of IRA in the semi-analytical model, which leads to some inconsistencies with the post-processing code, where this approximation is relaxed. Out of the seventeen selected candidates, we use in this work the eleven for which the post-processing technique can be ran self-consistently. The eleven galaxies that are used in the remainder of this work do represent the full range of star formation histories found in the Boötes I candidates. For all of these, the totality of the stars are formed *in situ*, i.e. there are not stars brought in the system through mergers. Mergers only provide gas to the system.

### 3.3 Inhomogeneous mixing

Most chemical evolution studies assume that the ejecta from dying stars are instantly cooled and mixed back into the ambient medium (*instantaneous mixing approximation*, IMA). Recchi et al. (2001) have shown that, indeed, most of the metals cool off in a few Myr if a low heating efficiency of a few per cent is adopted for SNe II. A rapid cooling of the metals would favor an efficient mixing with the ISM (but see Roy & Kunth 1995; Tenorio-Tagle 1996; Rieschick & Hensler 2003). In small systems, however, the stochastic sampling of the IMF introduced by the low star formation rates may lead to an internal dispersion in abundance ratios (Carigi & Hernandez 2008; Cescutti 2008).

In this study, chemical inhomogeneities are implemented by taking into account the empirical evidence that a strong correlation exists between the mean linear metallicity  $\bar{Z}$  and the intrinsic metallicity spread  $\sigma(Z)^2$  of Local Group dwarf galaxies and Galactic star clusters (Leaman 2012). At each time step, forming stars do not have all the same mean ISM metallicity,  $\bar{Z}$ . Rather, they follow a Gaussian distribution in  $Z$  values with

$$\log \sigma(Z)^2 = a + b \log(\bar{Z}), \quad (4)$$

where  $a = -0.6888970$  and  $b = 1.88930$  are derived from the slope of the relation for dwarf galaxies in figure 2 of Leaman (2012). The obvious boundary condition applies that stars do not form with negative metallicities. The detailed chemical composition is then obtained by scaling to the mean chemical mixture.

With this approach, we do not have to introduce further free parameters in order to deal with poorly known physical processes. Detailed three-dimensional hydrodynamical simulations are underway, that will allow us to better quantify the extent of chemical inhomogeneities in Boötes I and other UFDs in future papers.

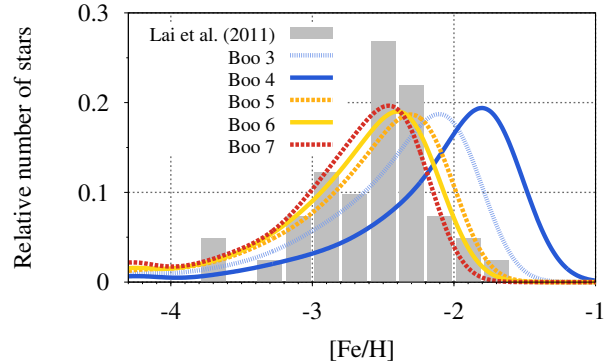


**Figure 1.** Theoretical (solid curves) and observed (histogram) MDFs of Boötes I. The observed MDF is the ‘combined’ MDF presented in Lai et al. (2011). The theoretical MDFs have been convolved with a Gaussian smoothing kernel of  $\sigma = 0.20$  dex, to take into account the random individual errors in  $[\text{Fe}/\text{H}]$  determinations.

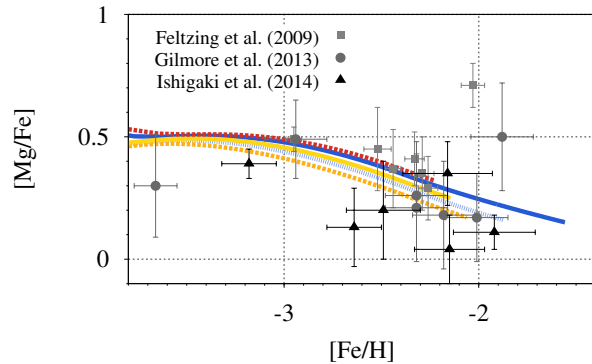


**Figure 2.** Theoretical  $[\text{Mg}/\text{Fe}]$  versus  $[\text{Fe}/\text{H}]$  for selected homogeneous chemical evolution models of Boötes I (coloured lines, colour coding is the same as in Fig. 1). Symbols refer to available high-resolution data (see Table 1).

## 4 RESULTS

In this section we discuss the model results in comparison with the available data. Furthermore, we provide some testable predictions, to be confirmed or disproved by future observations.

### 4.1 Homogeneous models

Within the homogeneous chemical evolution paradigm, we can address only *average* galaxy properties. Nevertheless, homogeneous models turn out to be very useful: because of the small computational demands, they allow a quick screening of the full parameter space, thus paving the way for more sophisticated, computationally expensive modelling. For the classical dwarf spheroidals –and also some UFDs– of the Local Group, it has been shown that the position of the peak of the stellar MDF, as well as the shape of its wings and the behaviour of the mean  $[\alpha/\text{Fe}]$  ratio as a function of  $[\text{Fe}/\text{H}]$ , sensibly constrain the star formation efficiency, gas accretion rate, IMF and occurrence of galactic winds in each galaxy (e.g. Lanfranchi & Matteucci 2004; Kirby et al. 2011; Vincenzo et al. 2014). The same observational constraints are used in the present study to

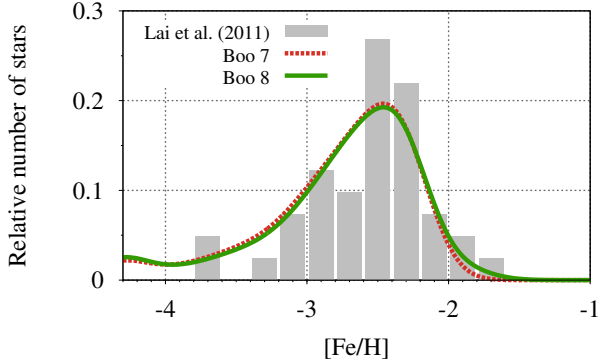


**Figure 3.** Same as Fig. 1, for models Boo 7 (red dashed line) and Boo 8 (green solid line). Model Boo 8 is the same as model Boo 7, except for a secondary star formation burst, extremely short but highly efficient, that is assumed to form a minority population of high- $[\alpha/\text{Fe}]$ , high metallicity stars.

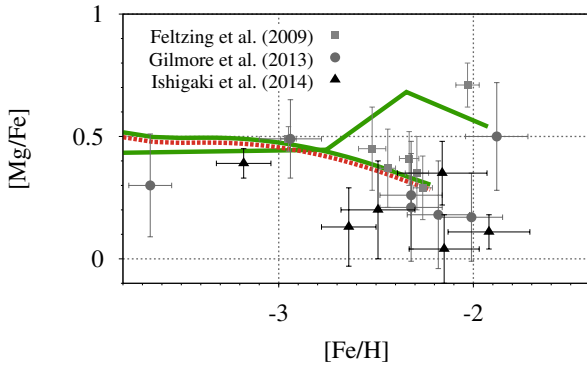


**Figure 4.** Same as Fig. 2 for models Boo 7 (red dashed line) and Boo 8 (green solid lines; each curve refers to a distinct star formation episode). The predictions of model Boo 7 have been shifted downward by 0.02 dex to make them clearly visible.

discriminate among different scenarios for the formation and evolution of Boötes I.

#### 4.1.1 Classical models

The adopted values of the input parameters for a subset of selected classical models are listed in Table 2 (columns 2 to 9), together with some of the model results (columns 10 to 13). We changed one by one the most important parameters of the simulation:

(i) As reviewed in the Introduction, current estimates of the dynamical mass of Boötes I enclosed within a half-light radius set lower limits to the total mass of the system that differ by more than one order of magnitude. We consider different amounts of dark matter in the models, ranging from null (model Boo 3) to  $\sim 10^8 M_\odot$  (models Boo 5–Boo 8). In general, we find that the lower the dark matter content, the higher the probability that SN explosions<sup>3</sup> destroy the system (this happens when SN explosions unbind all the gas), unless extremely low thermalization efficiencies of about 1

per cent are invoked (cf. models Boo 1 and Boo 2). However, our model Boo 3—with zero dark matter content—does not undergo disruption. This is due to the fact that, owing to its extremely shallow potential well, the gas heated by SN explosions escapes the system very early on ( $\Delta t_{\text{out}} = 275$  Myr; see Table 2, column 12), carrying away a considerable fraction of the thermal energy released by SNe before it can accumulate and destroy the system. While our treatment of SN feedback is clearly oversimplified and no firm conclusions can be drawn basing on the results of a single model, our findings provide some food for thought regarding the capability of small stellar systems without dark matter to survive multiple SN explosions.

(ii) At the beginning of the computation, the structure is assigned a baryon fraction,  $f_b = \mathcal{M}_b / \mathcal{M}_{\text{DM}}$ , varying from the cosmic fraction ( $f_b = 0.17 \pm 0.01$ ; Komatsu et al. 2009, model Boo 9) to  $f_b = 1$  (models Boo 1, Boo 2, Boo 4). This provides the mass to be accreted by infall (see Equation 1). The final baryon fraction is  $F_b = \mathcal{M}_{\text{stars}} / \mathcal{M}_{\text{DM}}$ , with  $\mathcal{M}_{\text{stars}}$  and  $\mathcal{M}_{\text{DM}}$  to be read from Table 2, columns 10 and 7, respectively. Notice that, in computing the final baryon fraction, we *assume* that the galaxy loses all of its gas by some external mechanism, such as tidal stripping and/or ram pressure stripping. We need to resort to an external mechanism (not implemented in the model) since feedback from SNe is not effective in removing all the neutral gas from the galaxy in our simulations, while the observations indicate that there is likely no H I in Boötes I today.

(iii) Color-magnitude diagrams reveal that the stellar population of Boötes I is old and has a small age spread. Resting on this piece of evidence, we test star formation histories consisting of one ancient burst, lasting 0.25, 0.5 or 1 Gyr. The star formation efficiency is fixed such as to predict a stellar mass of  $\sim 1.5\text{--}6 \times 10^4 M_\odot$  at the present time: the longer the duration of star formation, the lower must be the star formation efficiency.

(iv) Because of the very shallow potential wells considered in this study, only small heating efficiencies (of a few percent at most) can be tolerated for SNe and stellar winds. Otherwise, the galaxy gets destroyed at early epochs as a consequence of the energy released by the star formation activity.

(v) In order not to overestimate the mean metallicity of the stars, in the context of our models the infall time-scale has to be very short: most of the gas must be available since the very beginning of the computation to dilute the metals ejected by the first massive stars. We set  $\tau = 50$  Myr for all models.

In Fig. 1 we show the MDFs predicted by selected homogeneous models for Boötes I (the MDFs of models Boo 1, Boo 2 and Boo 3 overlap each other). The theoretical predictions are compared to the observed distribution of stars in the expanded sample of Lai et al. (2011). In Fig. 2 the run of  $[\text{Mg}/\text{Fe}]$  versus  $[\text{Fe}/\text{H}]$  is shown for the same models, in comparison with high-resolution data from different authors (we exclude Boo-119, for which Gilmore et al. 2013 measure  $[\text{Mg}/\text{Fe}] = 1.04$ ). All ratios are normalized using solar reference values from Asplund et al. (2009). All models assume one burst of star formation. While all the theoretical  $[\text{Mg}/\text{Fe}]$ – $[\text{Fe}/\text{H}]$  relations coarsely agree with the data, a satisfactory agreement with the observed MDF is obtained only for a subset of models, namely, the ones with the highest progenitor masses ( $\mathcal{M}_b \approx 10^7 M_\odot$ ;  $\mathcal{M}_{\text{DM}} = 6.5\text{--}11 \times 10^7 M_\odot$ ; see next paragraph). In the framework of the simple models considered here, the two stars with

<sup>3</sup> The number of SN explosions in the system is fixed by the observed stellar mass through a fiducial IMF.



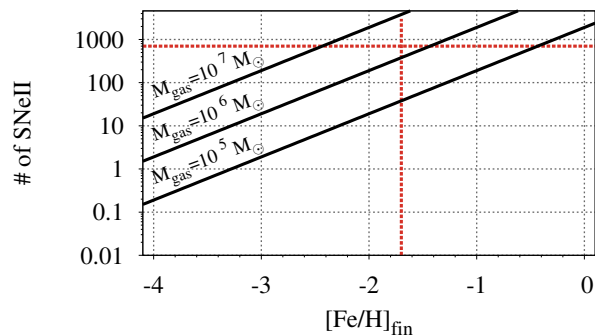


**Figure 5.** Number of SNeII necessary to reach  $[\text{Fe}/\text{H}]_{\text{fin}}$ , for different gas cloud masses (diagonals) in the absence of gas inflow/outflows. The horizontal dashed line marks the maximum number of SNeII that are expected to have exploded in Boötes I, while the vertical dashed line marks the maximum metallicity of Boötes I stars.

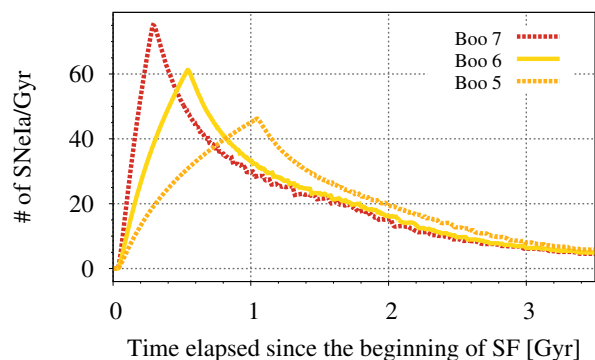


**Figure 6.** SNIa rates (in number of events per Gyr) as functions of the time elapsed since the beginning of the star formation predicted by models Boo 5, Boo 6 and Boo 7. The duration of the star formation is different in the three cases, namely it is 1, 0.5 and 0.25 Gyr, respectively.

$[\text{Mg}/\text{Fe}] \geq 0.5$  at  $[\text{Fe}/\text{H}] \geq -2.4$  can be explained only as forming in a second, short-lasting –but extremely efficient– starburst involving a minor fraction of unprocessed gas (see Figs. 3 and 4; see also Table 2, model Boo 8). Such an episode could be triggered by the interaction with the Milky Way.

The need for a substantially more massive progenitor can be easily understood. Let us assume that each core-collapse SN produces  $0.07 M_{\odot}$  of  $^{56}\text{Ni}$  (later decaying in  $^{56}\text{Fe}$ , Hamuy 2003) and that these ejecta fully mix within the considered volume. In such a hypothesis, and in the absence of inflow/outflow,  $<2$  SNI explosions already suffice to increase the metal content of a  $10^5 M_{\odot}$  gas cloud from  $[\text{Fe}/\text{H}] \simeq -4$  to  $[\text{Fe}/\text{H}] \simeq -3$ , while a metallicity  $[\text{Fe}/\text{H}] \simeq -2$  is reached after 19 such events. Since up to 700 SNeII are expected to have exploded in Boötes I (assuming a canonical IMF), we end up with the request that some  $10^6 M_{\odot}$  of gas must have been present in order to dilute the freshly produced metals

and not to shift the stellar MDF towards values higher than observed (see Fig. 5). We also note that some SNIa are expected to have exploded in the system while it was still forming stars (see Fig. 6). Since each SNIa releases  $0.6\text{--}0.8 M_{\odot}$  of Fe (Iwamoto et al. 1999), even more diluting gas is needed. Although the above discussion does not take into account the effect of large-scale outflows, that could efficiently remove most of the metals from active star-forming regions, nor the diluting effect of infall of unprocessed gas, it does give a good idea of the global magnitudes of gas needed to produce a Boötes I-like population.

It is also worth stressing that if the IMF is significantly different from what assumed here, our rough estimate changes. Weidner & Kroupa (2005) claim that steeper IMF slopes are to be expected for systems experiencing low star formation rates, which would result in a number of core-collapse SNe in Boötes I lower (or even significantly lower) than for a canonical IMF.

#### 4.1.2 Models in a cosmological context

In classical chemical evolution models, a number of free parameters are introduced in order to deal with poorly known physical processes such as gas condensation, star formation and supernova feedback, and the interaction with the environment is not taken into account. Semi-analytic models of galaxy formation coupled with  $N$ -body (dark matter only) cosmological simulations consider environmental effects to describe how gas (and stars) get into galaxies, thus removing the need for a most uncertain parameterization of the mass assembly histories of galaxies.

The (red) density map in Fig. 7 summarizes the results we get by post-processing for their detailed chemical properties eleven Boötes I candidates selected from the mock galaxy catalogue of Starkenburg et al. (2013, see Section 3.2). The theoretical distribution, that is normalized to its maximum value, shows where synthetic stars are most likely found in the  $[\text{Mg}/\text{Fe}]$  versus  $[\text{Fe}/\text{H}]$  plot. Superimposed are the relevant high-resolution abundance data (see Section 2). Overall, the model predictions agree with the observations within the errors, apart for a few very low- $[\text{Mg}/\text{Fe}]$  stars that are predicted by the models, but not observed. The Boötes I candidates are then inspected one-by-one; the lines in Fig. 7 show three representative models. Colour-coding refers to the star formation rate –the darker the curve, the higher the star formation rate. It is seen that the ‘blobs’ appearing in the density plot are not due to single star formation bursts but, rather, to the coaddition of different models. Indeed, each model spans almost the whole metallicity range of actual Boötes I stars. Some models can be rejected, as they clearly underestimate the  $[\text{Mg}/\text{Fe}]$  ratio at all metallicities (see the lower curve in Fig. 7, representative of this category of models), but the majority of them predict  $[\text{Mg}/\text{Fe}]$  ratios in reasonable to good agreement with the observations (e.g., middle and upper curves in Fig. 7). Looking back at the star formation and mass assembly histories predicted by the semi-analytic model, it is seen that:

(i) Models at odd with the observations display large cold gas masses (of the order of  $10^7 M_{\odot}$ ) and low star formation rates ( $<0.001 M_{\odot} \text{ yr}^{-1}$ ) at the epoch of chemical enrichment; as a consequence, their stellar ejecta are strongly diluted (see Fig. 5) and the predicted MDFs peak at  $[\text{Fe}/\text{H}]$  values lower than observed<sup>5</sup>.

<sup>4</sup> A high ratio of  $[\text{Mg}/\text{Fe}] = 0.71 \pm 0.09$  in Boo-127 (Feltzing et al. 2009) is not confirmed by successive investigations, that rather point to lower values,  $[\text{Mg}/\text{Fe}] = 0.17 \pm 0.18$  (Gilmore et al. 2013) or  $[\text{Mg}/\text{Fe}] = 0.11 \pm 0.07$  (Ishigaki et al. 2014).

<sup>5</sup> Notice that, following Starkenburg et al. (2013) and Li et al. (2010), in the models run in a fully cosmological setting only 5 per cent of the stellar ejecta is added directly to the cold gas component; the remainder is stored

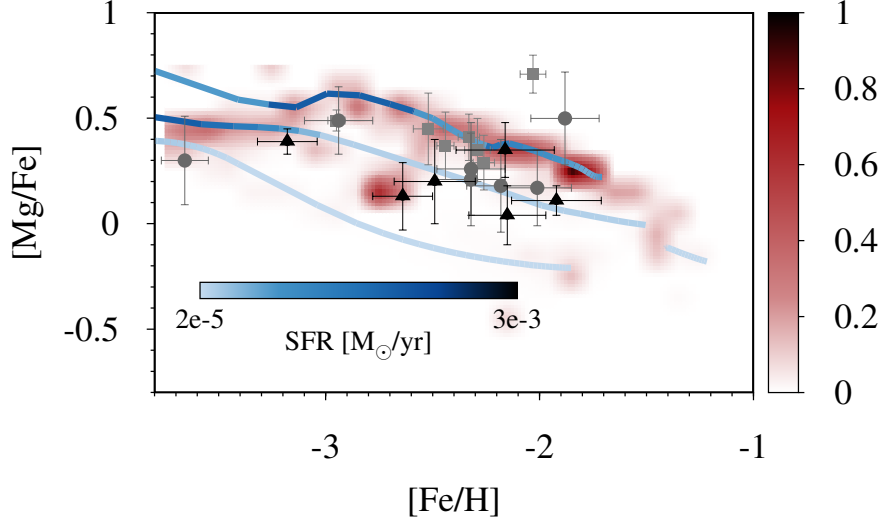


**Figure 7.**  $[\text{Mg}/\text{Fe}]$  versus  $[\text{Fe}/\text{H}]$  for the models run in a full cosmological context. The density map shows the distribution of long-lived stars for eleven Boötes I candidates selected from the Starkenburg et al. (2013) mock catalogue of Milky Way’s satellites. The distribution is normalized to its maximum value. The curves show the predictions of three representative models, colour-coded according to their star formation rates (legend at the bottom of the plot). Symbols with error bars are high-resolution data for giant stars in Boötes I from Feltzing et al. (2009; squares), Gilmore et al. (2013; circles) and Ishigaki et al. (2014; triangles).

(ii) A good fit to the observed properties is obtained when accretion and/or loss of matter properly compensate for the star formation activity; this delicate balance is achieved by a few models.

#### 4.2 Inhomogeneous models

In Figs. 8 and 9 we show the behaviour of several abundance ratios as a function of  $[\text{Fe}/\text{H}]$  predicted by two of our classical models, model Boo5 and model Boo7 (left and right panels in each figure, respectively), when chemical inhomogeneities are implemented following the empirical relation between mean metallicity and intrinsic metallicity spread found for local dwarf galaxies by Leaman (2012; see Section 3.3). These two models have been chosen since they predict the lowest (model Boo5) and highest (model Boo7)  $[\text{Mg}/\text{Fe}]$  ratios at any given  $[\text{Fe}/\text{H}]$ , while their MDFs both agree reasonably well with the observational data.

In model Boo5 the star formation is less efficient –and lasts longer– than in model Boo7. Therefore, in model Boo5 the ISM gets significantly enriched in iron by SNeIa, at variance with model Boo7. This results in lower element-to-iron ratios for  $[\text{Fe}/\text{H}] > -2.5$  for all elements, in better agreement with the bulk of the observations. A relatively long-lasting star formation seems, hence, favoured in the frame of our models. Also, the spread in the abundance ratios is reasonably well reproduced, with the notable exception of carbon. It has been suggested (Gilmore et al. 2013, and references therein) that this element might suffer a complex evolutionary history, with two distinct enrichment channels active at very low metallicities. This would explain both the CEMP-no

and the carbon-normal stars in Boötes I. A detailed study of carbon evolution should consider the two different enrichment paths and is beyond the scope of the present paper.

There are a few stars with anomalous abundances in one or more elements other than carbon that can not be explained by our models:

(i) Boo-119: this star has  $[\text{Na}/\text{Fe}] = 0.73 \pm 0.23$ ,  $[\text{Mg}/\text{Fe}] = 1.04 \pm 0.22$ ,  $[\text{Ti}/\text{Fe}] = 0.80 \pm 0.28$  (Gilmore et al. 2013). None of these values can be explained by our models. Yet,  $[\text{Ca}/\text{Fe}]$  is normal in this star ( $\sim 0.45$  dex).

(ii) Boo-127: our models can not account for the high magnesium-to-iron ratio,  $[\text{Mg}/\text{Fe}] = 0.71 \pm 0.09$ , measured by Feltzing et al. (2009). However, if  $[\text{Mg}/\text{Fe}] = 0.17 \pm 0.18$ , as suggested by Gilmore et al. (2013), or  $[\text{Mg}/\text{Fe}] = 0.11 \pm 0.07$  (Ishigaki et al. 2014) our models can reproduce the data. The Na abundance measured by Ishigaki et al. (2014) for this star,  $[\text{Na}/\text{Fe}] = -0.18 \pm 0.15$ , is also well explained by the models.

(iii) Boo-41 and Boo-1137: both have  $[\text{Ti}/\text{Fe}] > 0.45$  dex, well in excess of the values predicted by our models, even when accounting for the fact that the adopted Ti yields severely underestimate the trend of  $[\text{Ti}/\text{Fe}]$  versus  $[\text{Fe}/\text{H}]$  for Galactic halo stars (see Romano et al. 2010, their figure 22).

(iv) Boo-117, Boo-127 and Boo-911: the nearly solar  $[\text{Ca}/\text{Fe}]$  ratios reported by Feltzing et al. (2009) for Boo-127 and Ishigaki et al. (2014) for the other two objects can not be explained by our models. However, higher ratios have been reported, that better match the model predictions.

in a hot ejected component, from which may or may not be re-accreted by the system.

Fig. 10 shows the MDFs predicted by models Boo5 and Boo7 when chemical inhomogeneities are implemented in the code (dashed lines). Adding the inhomogeneities leads to wider theo-



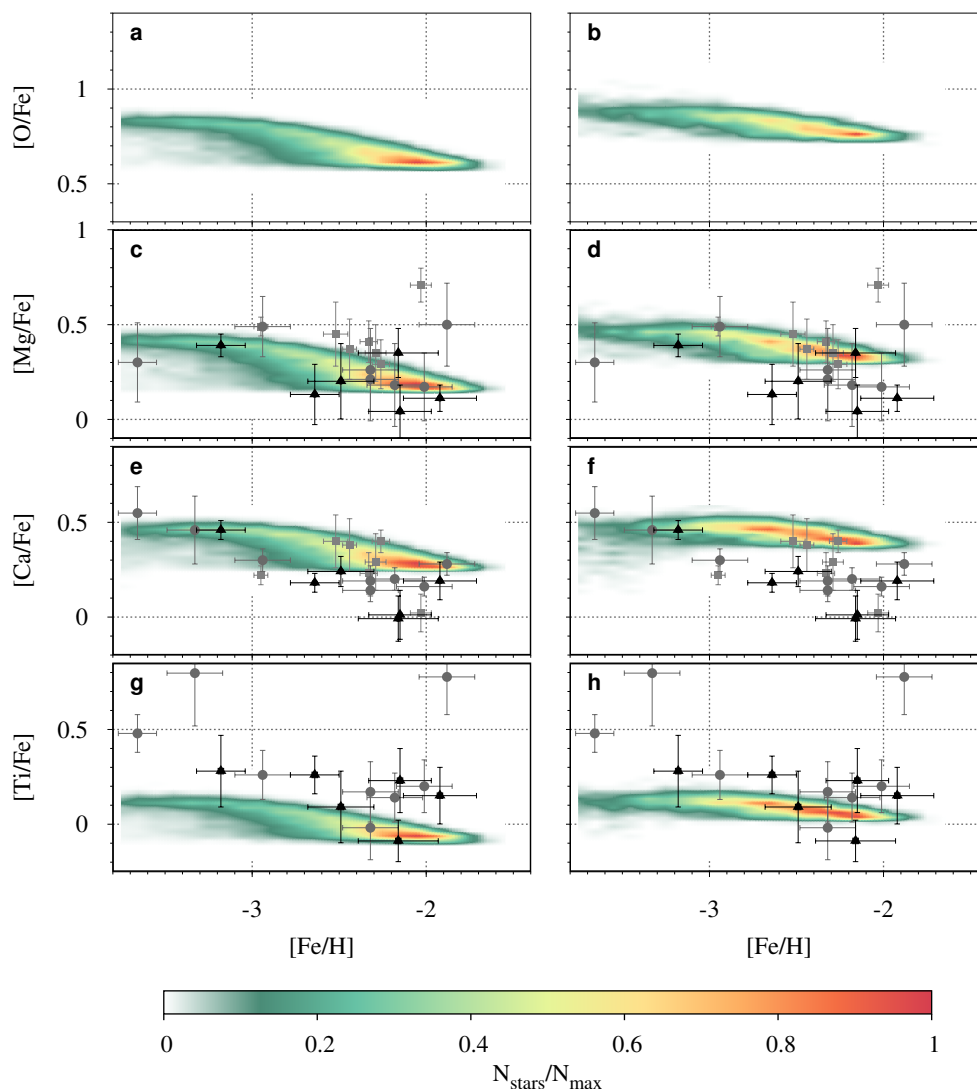


**Figure 8.**  $[X/Fe]$  versus  $[Fe/H]$  for  $X = O$  (panels a, b),  $Mg$  (panels c, d),  $Ca$  (panels e, f) and  $Ti$  (panels g, h). The density maps show the distributions of long-lived stars for models Boo 5 (left panels) and Boo 7 (right panels) when chemical inhomogeneities are implemented following Leaman’s (2012) empirical relation between mean metallicity and metallicity spread. Each distribution is normalized to its maximum value. Superimposed are high-resolution data for giant stars in Boötes I (squares: Feltzing et al. 2009; circles: Gilmore et al. 2013; triangles: Ishigaki et al. 2014).

retical MDFs (cfr. Fig. 1), that are still broadly consistent with the observed distribution (grey histogram).

We close this section with a note of caution. Combining data sets from different authors, all coming with their different, methodology-dependent systematics, may result in overestimating the intrinsic abundance dispersions, if not even detecting spurious abundance spreads. The homogeneous analysis of a statistically significant sample of Boötes I stars is badly needed to shed light on important issues such as the existence and significance of abundance spreads and the role of SNe Ia in enriching the ISM of Boötes I, one of the smallest known Milky Way companions.

## 5 SUMMARY AND CONCLUSIONS

The choice of Boötes I as a case of study was dictated by several reasons. First, while it has a total luminosity nearly ten times smaller than the faintest classical dwarfs, it is still one of the brightest among the so-called UFDs ( $L_V = 2.8 \times 10^4 M_\odot$ , also in the range

of globular clusters). The separation in two classes of the dwarf satellites discovered before and after the advent of the Sloan Digital Sky Survey (SDSS; York et al. 2000) is probably an arbitrary one (see, e.g., Belokurov 2013); still we are interested to the chemical evolution of stellar systems that, at face value, have a total stellar mass far too low to retain the SN ejecta (say, lower than  $10^6 M_\odot$ ). On the other hand, the smaller the total stellar mass of a system, the lower the total number of stars, and, in particular, of stars suitable for chemical analysis (i.e. red giant branch stars, in the range of distances of dwarf satellites of the Milky Way). In this framework Boötes I appears as a good trade-off system, with the additional advantage of being relatively nearby. Probably, because of the above characteristics it is also among the best studied UFDs, in particular from the spectroscopic point of view (see Section 2). Hence, relatively abundant observational constraints are available for comparison with chemical evolution models. Finally, the galaxy is completely dominated by very old stars with a small spread in age (de Jong et al. 2008; Hughes et al. 2008)), hence the star formation history is quite simple.

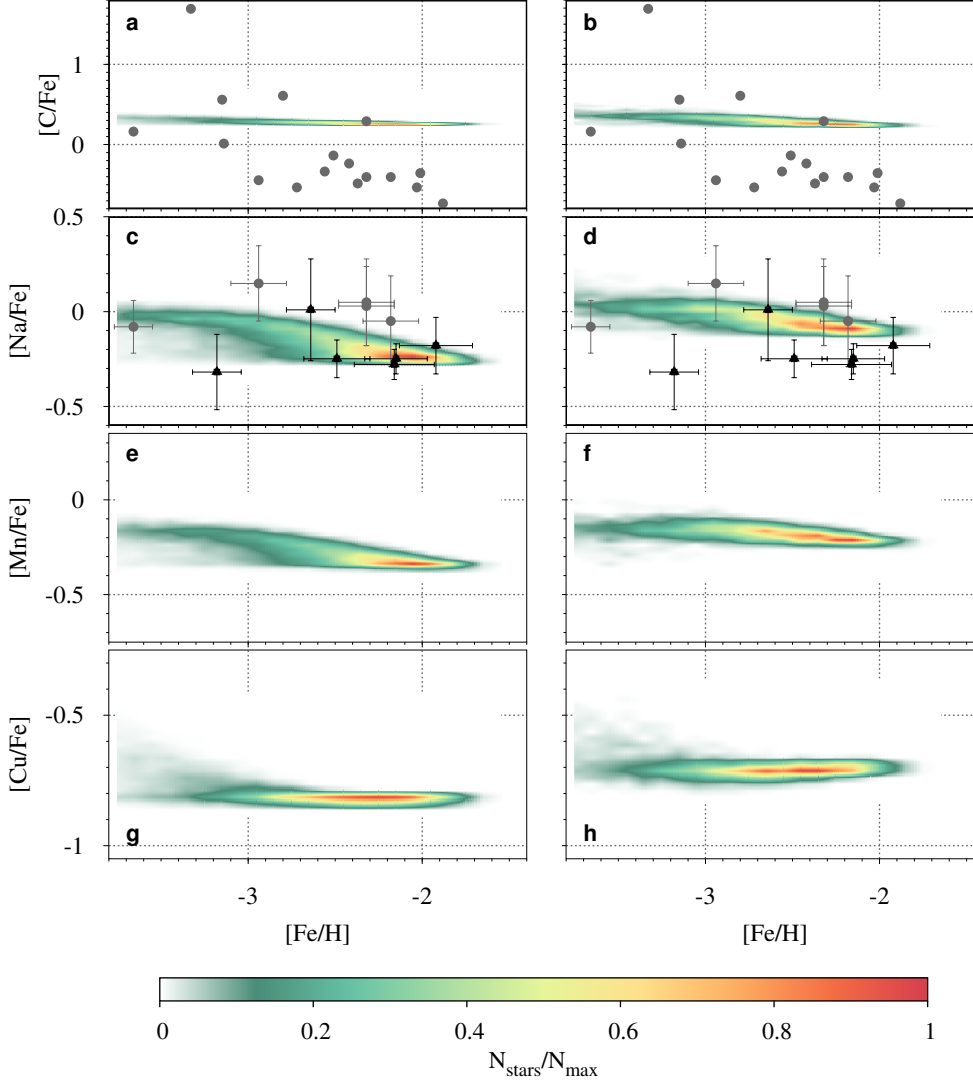


**Figure 9.** Same as Fig. 8 for C (panels a, b), Na (panels c, d), Mn (panels e, f) and Cu (panels g, h). Carbon data from Norris et al. (2010a) and Lai et al. (2011, one star).

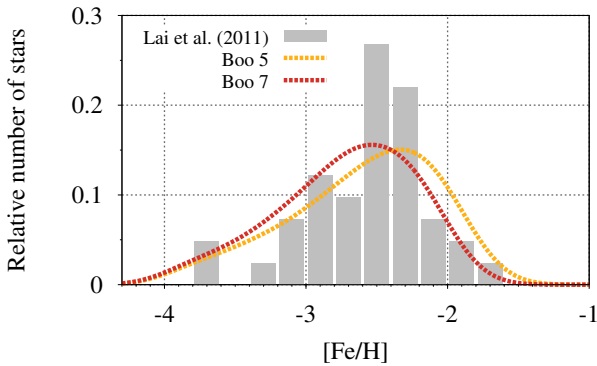


**Figure 10.** Theoretical MDFs (dashed lines) predicted by models Boö 5 and Boö 7 when chemical inhomogeneities are implemented, compared to the observed one (histogram).

We have run and compared different chemical evolution models for Boötes I—classical models versus models run in a fully cos-

mological setting, as well as homogeneous versus inhomogeneous models—and compared the model predictions with the available observations.

(i) As for the classical models, we suggest, in agreement with Vincenzo et al. (2014), that Boötes I must have formed through accretion of relatively large amounts of gas ( $\mathcal{M}_b \approx 10^7 M_\odot$ ) on very short time scales ( $\tau = 50$  Myr) and converted into stars less than 1 per cent of its baryons (see also Salvadori & Ferrara 2009). These conditions have to be met in order not to overestimate the metal content of Boötes I stars. In the case of the cosmologically-motivated models, lower amounts of diluting gas are needed, because most of the stellar ejecta is stored in a hot ejected component, rather than being mixed directly with the neutral ISM.

(ii) At variance with Vincenzo et al. (2014), we do not find a clear-cut evidence that the gas left over from the star formation process can be expelled from the galaxy through large-scale outflows; rather, in the classical approach we are left with huge amounts of gas and have to turn to the cosmologically-motivated models to find that the residual gas is most likely stripped by the interaction with the Milky Way.

(iii) Though some of the cosmologically-motivated models predict lower than observed  $[\alpha/\text{Fe}]$  ratios in Boötes I, the majority of them provide reasonable to good fit to the available data. Looking back at the star formation and mass assembly histories predicted by the semi-analytical model, we find that a delicate balance of mass loss, mass accretion and star formation is needed for the model predictions to agree with the observations.

(iv) Chemical inhomogeneities are implemented in our code following the empirical relation between mean metallicity and metallicity spread found by Leaman (2012) for dwarf galaxies in the Local Group. In this framework, our capability to reproduce the observed spread in abundance ratios is directly linked to the extent of the variation of the relative yields with metallicity that is expected owing to the adopted stellar nucleosynthesis prescriptions (see Appendix A).

(v) Full (three-dimensional) hydrodynamical simulations including stellar feedback and chemical enrichment are needed in order to obtain better insights on issues such as the development of outflows and the establishment of inhomogeneities in Boötes I; we have recently embarked on this kind of computations.

As a final remark, it is worth stressing that at present high-resolution spectroscopic observations have been obtained only for a small sample of Boötes I stars. This severely hampers our capability of drawing firm conclusions on issues such as the impact of SNeIa in enriching the ISM of Boötes I, or the significance of inhomogeneities.

## ACKNOWLEDGEMENTS

The authors are indebted to the Virgo Consortium, which was responsible for designing and running the halo simulations of the Aquarius Project. Additionally, they are grateful to Gabriella De Lucia, Amina Helmi and Yang-Shyang Li for their role in developing the semi-analytic model of galaxy formation used in this paper. DR thanks Francesca Matteucci for countless discussions on chemical evolution and wise advice. Finally, we wish to thank the anonymous referee for comments that improved the presentation of the paper. DR and ES are indebted to the International Space Science Institute (ISSI), Bern, Switzerland, for supporting and funding the international team “First stars in dwarf galaxies”. MB and DR acknowledge financial support from PRIN MIUR 2010–2011, project “The Chemical and Dynamical Evolution of the Milky Way and Local Group Galaxies”, prot. 2010LY5N2T. DR acknowledges support from PRIN INAF 2010, project “Looking for the elusive building blocks of the Milky Way and Andromeda Halos”. RL acknowledges financial support to the DAGAL network from the People Programme (Marie Curie Actions) of the European Union’s Seventh Framework Programme FP7/2007– 2013/ under REA grant agreement number PITN-GA-2011-289313. ES gratefully acknowledges the Canadian Institute for Advanced Research (CIAR) Global Scholar Academy for support.

## REFERENCES

Asplund M., Grevesse N., Sauval A. J., Scott P., 2009, *ARA&A*, 47, 481  
 Bailin J., Ford A., 2007, *MNRAS*, 375, L41  
 Battaglia G., et al., 2006, *A&A*, 459, 423  
 Belokurov V., 2013, *New Astron. Rev.*, 57, 100  
 Belokurov V., et al., 2006, *ApJ*, 647, L111

Bradamante F., Matteucci F., D’Ercole A., 1998, *A&A*, 337, 338  
 Carigi L., Hernandez X., 2008, *MNRAS*, 390, 582  
 Carretta E., Bragaglia A., Gratton R., D’Orazi V., Lucatello S., 2009, *A&A*, 508, 695  
 Cescutti G., 2008, *A&A*, 481, 691  
 Conselice C. J., 2012, preprint (arXiv:1212.5641)  
 Cooper A. P., et al., 2010, *MNRAS*, 406, 744  
 Croton D. J., Springel V., White S. D. M., De Lucia G., Frenk C. S., Gao L., Jenkins A., Kauffmann G., Navarro J. F., Yoshida N., 2006, *MNRAS*, 365, 11  
 de Jong J. T. A., Rix H.-W., Martin N. F., Zucker D. B., Dolphin A. E., Bell E. F., Belokurov V., Evans N. W., 2008, *AJ*, 135, 1361  
 De Lucia G., Blaizot J., 2007, *MNRAS*, 375, 2  
 De Lucia G., Helmi A., 2008, *MNRAS*, 391, 14  
 De Lucia G., Kauffmann G., White S. D. M., 2004, *MNRAS*, 349, 1101  
 De Lucia G., Tornatore L., Frenk C. S., Helmi A., Navarro J. F., White S. D. M., 2014, *MNRAS*, 445, 970  
 Desai V., Dalcanton J. J., Reed D., Mayer L., Quinn T., Governato F., 2004, *MNRAS*, 351, 265  
 Feltzing S., Eriksson K., Kleya J., Wilkinson M. I., 2009, *A&A*, 508, L1  
 Font A. S., et al., 2011, *MNRAS*, 417, 1260  
 Fulbright J. P., Rich R. M., Castro S., 2004, *ApJ*, 612, 447  
 Gibson B. K., 1994, *MNRAS*, 271, L35  
 Gilmore G., Norris J. E., Monaco L., Yong D., Wyse R. F. G., Geisler D., 2013, *ApJ*, 763, 61  
 Gratton R., Sneden C., Carretta E., 2004, *ARA&A*, 42, 385  
 Hamuy M., 2003, *ApJ*, 582, 905  
 Hughes J., Wallerstein G., Bossi A., 2008, *AJ*, 136, 2321  
 Ishigaki M. N., Aoki W., Arimoto N., Okamoto S., preprint (arXiv:1401.1265)  
 Iwamoto K., Brachwitz F., Nomoto K., Kishimoto N., Umeda H., Hix W. R., Thielemann F.-K., 1999, *ApJS*, 125, 439  
 Karakas A. I., 2010, *MNRAS*, 403, 1413  
 Kauffmann G., Colberg J. M., Diaferio A., White S. D. M., 1999, *MNRAS*, 307, 529  
 Kennicutt R. C. Jr., 1998, *ApJ*, 498, 541  
 Kirby E. N., et al., 2010, *ApJS*, 191, 352  
 Kirby E. N., Lanfranchi G. A., Simon J. D., Cohen J. G., Guhathakurta P., 2011, *ApJ*, 727, 78  
 Kobayashi C., Umeda H., Nomoto K., Tominaga N., Ohkubo T., 2006, *ApJ*, 653, 1145  
 Koch A., McWilliam A., Grebel E. K., Zucker D. B., Belokurov V., 2008, *ApJ*, 688, L13  
 Komatsu E., et al., 2009, *ApJS*, 180, 330  
 Koposov S. E., et al., 2011, *ApJ*, 736, 146  
 Kroupa P., 2001, *MNRAS*, 322, 231  
 Lai D. K., Lee Y. S., Bolte M., Lucatello S., Beers T. C., Johnson J. A., Sivarani T., Rockosi C. M., 2011, *ApJ*, 738, 51  
 Lanfranchi G. A., Matteucci F., 2004, *MNRAS*, 351, 1338  
 Leaman R., 2012, *AJ*, 144, 183  
 Li Y.-S., De Lucia G., Helmi A., 2010, *MNRAS*, 401, 2036  
 Marcolini A., D’Ercole A., Brighenti F., Recchi S., 2006, *MNRAS*, 371, 643  
 Marconi G., Matteucci F., Tosi M., 1994, *MNRAS*, 270, 35  
 Martin C. L., Kobulnicky H. A., Heckman T. M., 2002, *ApJ*, 574, 663  
 Martin N. F., Ibata R. A., Chapman S. C., Irwin M., Lewis G. F., 2007, *MNRAS*, 380, 281  
 Matteucci F., 2001, *The chemical evolution of the Galaxy. Astro-*

- physics and Space Science Library. Kluwer Academic Publishers, Dordrecht
- Matteucci F., 2012, Chemical evolution of galaxies. Springer-Verlag Berlin, Heidelberg
- Matteucci F., Greggio L., 1986, *A&A*, 154, 279
- Mayer L., Mastropietro C., Wadsley J., Stadel J., Moore B., 2006, *MNRAS*, 369, 1021
- McConnachie A. W., 2012, *AJ*, 144, 4
- Melioli C., de Gouveia Dal Pino E. M., 2004, *A&A*, 424, 817
- Mori M., Burkert A., 2000, *ApJ*, 538, 559
- Norris J. E., Gilmore G., Wyse R. F. G., Wilkinson M. I., Belokurov V., Evans N. W., Zucker D. B., 2008, *ApJ*, 689, L113
- Norris J. E., Wyse R. F. G., Gilmore G., Yong D., Frebel A., Wilkinson M. I., Belokurov V., Zucker D. B., 2010a, *ApJ*, 723, 1632
- Norris J. E., Yong D., Gilmore G., Wyse R. F. G., 2010b, *ApJ*, 711, 350
- Oke J. B., et al., 1995, *PASP*, 107, 375
- Pagel B. E. J., 1997, *Nucleosynthesis and Chemical Evolution of Galaxies*. Cambridge Univ. Press, Cambridge
- Recchi S., 2014, *Advances in Astronomy*, Vol. 2014, Article ID 750754
- Recchi S., Hensler G., 2013, *A&A*, 551, A41
- Recchi S., Matteucci F., D’Ercole A., 2001, *MNRAS*, 322, 800
- Rieschick A., Hensler G., 2003, *Ap&SS*, 284, 861
- Romano D., Starkenburg E., 2013, *MNRAS*, 434, 471
- Romano D., Karakas A. I., Tosi M., Matteucci F., 2010, *A&A*, 522, A32
- Roy J.-R., Kunth D., 1995, *A&A*, 294, 432
- Salpeter E. E., 1955, *ApJ*, 121, 161
- Salvadori S., Ferrara A., 2009, *MNRAS*, 395, L6
- Sawala T., et al., 2014, preprint (arXiv:1406.6362)
- Sawala T., Scannapieco C., Maio U., White S., 2010, *MNRAS*, 402, 1599
- Schmidt M., 1959, *ApJ*, 129, 243
- Silich S. A., Tenorio-Tagle G., 1998, *MNRAS*, 299, 249
- Springel V., White S. D. M., Tormen G., Kauffmann G., 2001, *MNRAS*, 328, 726
- Springel V., Wang J., Vogelsberger M., Ludlow A., Jenkins A., Helmi A., Navarro J. F., Frenk C. S., White S. D. M., 2008, *MNRAS*, 391, 1685
- Starkenburg E., et al., 2013, *A&A*, 549, A88
- Sutherland R. S., Dopita M. A., 1993, *ApJS*, 88, 253
- Tenorio-Tagle G., 1996, *AJ*, 111, 1641
- Tinsley B. M., 1980, *Fundam. Cosm. Phys.*, 5, 287
- Vader J. P., 1986, *ApJ*, 305, 669
- Vader J. P., 1987, *ApJ*, 317, 128
- van den Hoek L. B., Groenewegen M. A. T., 1997, *A&AS*, 123, 305
- Vargas L. C., Geha M., Kirby E. N., Simon J. D., 2013, *ApJ*, 767, 134
- Vincenzo F., Matteucci F., Vattakunnel S., Lanfranchi G. A., *MNRAS*, 441, 2815
- Wang B., 1995, *ApJ*, 444, 590
- Weidner C., Kroupa P., 2005, *ApJ*, 625, 754
- Wolf J., Martinez G. D., Bullock J. S., Kaplinghat M., Geha M., Munoz R. R., Simon J. D., Avedo F. F., 2010, *MNRAS*, 406, 1220
- Woosley S. E., Weaver T. A., 1995, *ApJS*, 101, 181
- York D. G., et al., 2000, *AJ*, 120, 1579

## APPENDIX A: THE IMPACT OF THE CHOICE OF THE STELLAR YIELDS

In Fig. 11 we show the predictions of model Boo7 with chemical inhomogeneities implemented as described in Sect. 3.3, for a different choice of the stellar yields, namely, Karakas (2010) for single low- and intermediate-mass stars and Kobayashi et al. (2006) for single massive stars exploding as SNeII (see Sect. 3.1.3). When comparing the results shown in Fig. 11 with the corresponding ones relevant to our standard yield choice, displayed in the right-hand panels of Figs. 8 and 9, it is immediately seen that with the new nucleosynthesis prescriptions:

- (i) the bulk of the synthetic stars has higher metallicities;
- (ii) lower  $[X/Fe]$  ratios are predicted at all  $[Fe/H]$  for C, Na, O, Ca, Ti, Mn, and Cu, while the predicted  $[Mg/Fe]$  ratio is slightly higher for  $[Fe/H] \geq -2$  dex;
- (iii) a much smaller dispersion is expected for all the abundance ratios, with the notable exception of  $[O/Fe]$ .

The first two points simply reflect the fact that lower/higher amounts of each chemical element are restored to the ISM by dying stars according to the different nucleosynthesis studies analysed here. The third issue, instead, has to do with the variation of the relative yields with metallicity, that for Kobayashi et al. (2006) is smaller than for Woosley & Weaver (1995), at least for the metallicity range probed by this study.

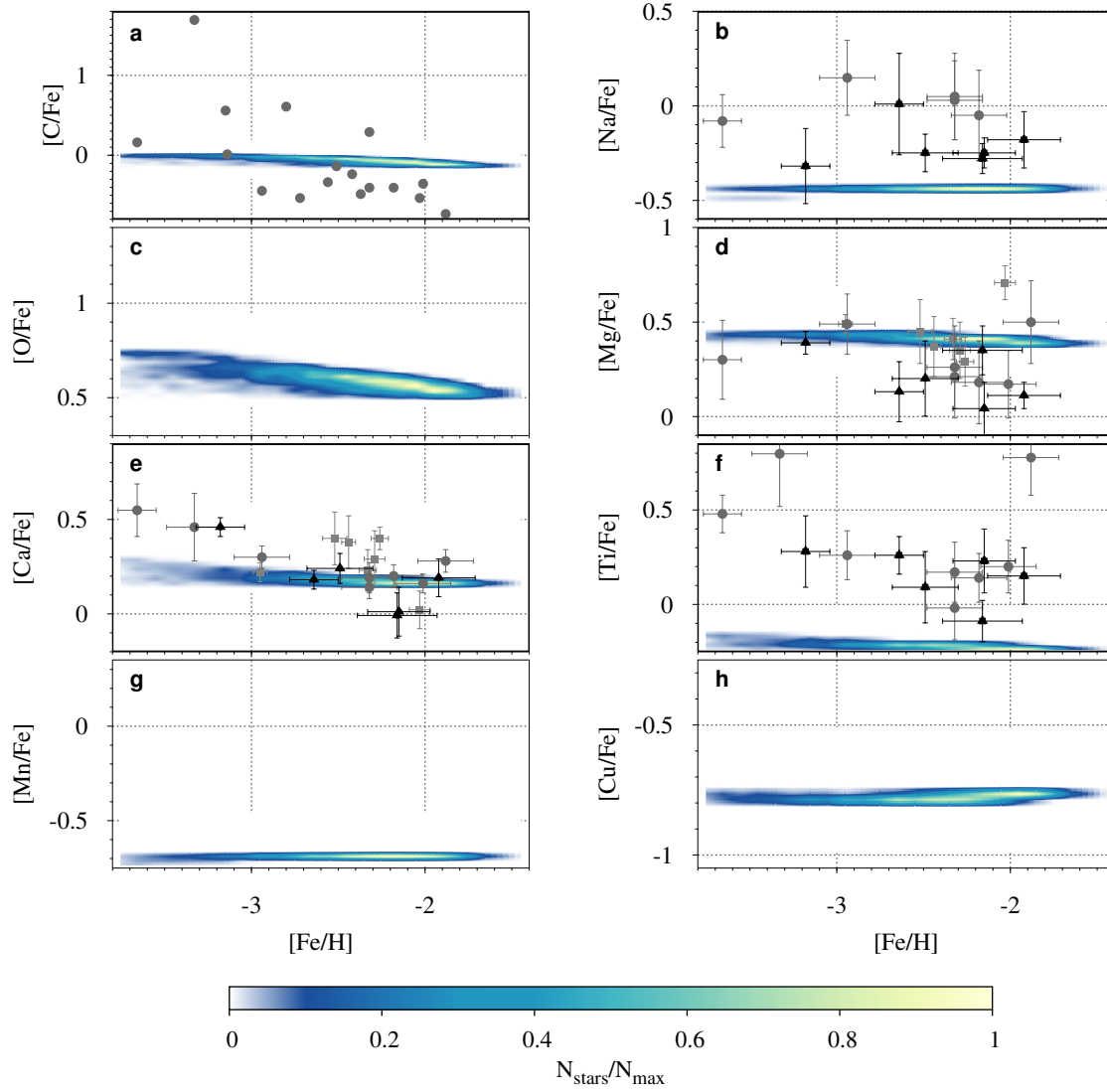


**Figure 11.**  $[X/Fe]$ – $[Fe/H]$  relations in Boötes I. The contours show the frequency distribution of long-lived stars in the simulated galaxy, where yellow is for the highest frequency and blue for the lowest one. High-resolution data for giant stars are taken from Feltzing et al. (2009; squares), Gilmore et al. (2013; circles) and Ishigaki et al. (2014; triangles).